

University of Groningen

## On the Self-Repair of WS<sub>2</sub>/a-C Tribocoating

Cao, Huatang; Wen, Feng; De Hosson, Jeff Th. M.; Pei, Yutao

*Published in:*  
Advanced Materials Interfaces

*DOI:*  
[10.1002/admi.201900938](https://doi.org/10.1002/admi.201900938)

**IMPORTANT NOTE: You are advised to consult the publisher's version (publisher's PDF) if you wish to cite from it. Please check the document version below.**

*Document Version*  
Publisher's PDF, also known as Version of record

*Publication date:*  
2020

[Link to publication in University of Groningen/UMCG research database](#)

*Citation for published version (APA):*

Cao, H., Wen, F., De Hosson, J. T. M., & Pei, Y. (2020). On the Self-Repair of WS<sub>2</sub>/a-C Tribocoating. *Advanced Materials Interfaces*, 7(1), [1900938]. <https://doi.org/10.1002/admi.201900938>

**Copyright**

Other than for strictly personal use, it is not permitted to download or to forward/distribute the text or part of it without the consent of the author(s) and/or copyright holder(s), unless the work is under an open content license (like Creative Commons).

**Take-down policy**

If you believe that this document breaches copyright please contact us providing details, and we will remove access to the work immediately and investigate your claim.

*Downloaded from the University of Groningen/UMCG research database (Pure): <http://www.rug.nl/research/portal>. For technical reasons the number of authors shown on this cover page is limited to 10 maximum.*

# On the Self-Repair of WS<sub>2</sub>/a-C Tribocoating

Huatang Cao, Feng Wen, Jeff Th. M. De Hosson, and Yutao Pei\*

**This study investigates the self-healing capacity of a WS<sub>2</sub>/amorphous carbon (a-C) tribocoating. It is found that prenotches up to 45 μm wide in the WS<sub>2</sub>/a-C coating surface can be completely healed under the stimulus of sliding operations. The in situ tribotest of 100, 500, 2000, and 6000 laps confirms a dynamic filling of tribofilms that patch the voids and prenotched damages. The stabilized coefficient of friction (CoF) remains at an ultralow value down to 0.02, independent of the prenotched damage at the top of coating. The sites of notched damage in fact act as lubricant reservoirs to accumulate the otherwise “wasted” debris, which are restored as a superlubricant by the sliding operation. High resolution transmission electron microscopy reveals that WS<sub>2</sub> (002) nanoplatelets in the healed notch are parallel to the top coating surface but conformal to the coating/notch interface. The patchy tribofilm holds excellent promise for the self-repair of damages in the field of tribology.**

## 1. Introduction

During their use in service, materials accumulate defects which may lead to critical damage accumulation and catastrophic failure. If advanced materials could counter degradation through the initiation of an intrinsic repair mechanism that responds to damages occurring during applications in practice, the production costs could be reduced drastically, with substantial savings of material resources and energy.<sup>[1]</sup> Self-healing materials may also stretch the safety margins for the design of mechanically, thermally and chemically exposed components in various technical domains, which, in turn, would streamline

component construction. As a result, self-healing materials are attracting growing attention and have been significantly developed during the last decade.

At present, however, self-healing phenomena do not appear intrinsically and autonomously in materials but usually thanks to a subsequent extrinsic trigger based on external thermal, mechanical, electrical, and optical stimuli, or a combination of them. Self-healing was introduced by White et al.<sup>[2]</sup> into polymer composites, where embedded prefilled microcapsules rupture during mechanical loading, subsequently releasing a liquid healing agent toward the crack sites by a capillary action. The contact between healing agent and catalyst triggers

polymerization to bridge and close the fissure. Further approaches to achieve self-healing functionality were evolving various approaches such as polymer crosslinking,<sup>[3]</sup> microbacterial healing,<sup>[4,5]</sup> and high-temperature induced ceramic oxidation.<sup>[6,7]</sup> However, in the realm of friction and wear, there is little information on the self-healing potential in tribocoatings. It is known that triboinduced wear is damaging and gradual removal of materials leading to wear debris.


In triboapplications, initial cracks may run along columnar boundaries, branch and induce catastrophic flaking or spalling of sputtered tribocoatings. This may result in sudden failures. Considerable efforts, e.g., employing an interlayer between coating and substrate,<sup>[8]</sup> tuning the deposition distance,<sup>[9]</sup> controlling the microstructure,<sup>[10–12]</sup> doping with other elements,<sup>[13–15]</sup> as well as design of multilayered structure,<sup>[16,17]</sup> have been devoted to improving the mechanical integrity of coatings and substrate systems under various conditions. In particular, nanocomposite coatings have been designed to be tough enough to resist the nucleation and propagation of cracks under severe stresses or a high energy absorbance has often been adopted to suppress crack propagation.<sup>[12,18–20]</sup> However, to date it turned out in reality improbable to produce completely flawless coatings.

One approach to reduce wear could be to enhance lubrication, for example by applying transition metal dichalcogenides (TMDs) such as WS<sub>2</sub> and MoS<sub>2</sub>, which are recognized as outstanding solid lubricants widely used in aerospace applications.<sup>[21–23]</sup> Their intrinsic lubricating property is attributed to the anisotropic crystallographic structure and atomic bonding characteristics. TMDs are in fact hexagonal lamellar compounds with layers of tungsten or molybdenum atoms sandwiched in between the layers of packed sulfur atoms. Each unit is characterized by strong covalent bonds, whereas the sandwiched layers are coupled via weak van der Waals interactions.<sup>[24–27]</sup> The ultralow shear strength ( $\tau = 1\text{--}2$  MPa) in (002) basal orientation allows each WS<sub>2</sub> unit to easily glide along the sliding

Dr. H. T. Cao, Prof. F. Wen, Prof. Y. T. Pei  
 Department of Advanced Production Engineering  
 Engineering and Technology Institute Groningen  
 University of Groningen  
 Nijenborgh 4, 9747 AG Groningen, The Netherlands  
 E-mail: y.pei@rug.nl

Prof. F. Wen  
 School of Materials Science and Engineering  
 Hainan University  
 Haikou 570228, P. R. China

Prof. J. Th. M. De Hosson  
 Department of Applied Physics  
 Zernike Institute for Advanced Materials  
 University of Groningen  
 Nijenborgh 4, 9747 AG Groningen, The Netherlands

 The ORCID identification number(s) for the author(s) of this article can be found under <https://doi.org/10.1002/admi.201900938>.

© 2019 The Authors. Published by WILEY-VCH Verlag GmbH & Co. KGaA, Weinheim. This is an open access article under the terms of the Creative Commons Attribution-NonCommercial-NoDerivs License, which permits use and distribution in any medium, provided the original work is properly cited, the use is non-commercial and no modifications or adaptations are made.

DOI: 10.1002/admi.201900938

interfaces leading to an ultralow friction.<sup>[21]</sup> Other studies also proposed that the localized charge induced Coulombic repulsion between TMD layers might play a key role in reducing friction.<sup>[28]</sup> Accordingly, WS<sub>2</sub> or MoS<sub>2</sub> is favorably introduced into tribocoatings prepared by vacuum deposition methods such as magnetron sputtering<sup>[29,30]</sup> and laser ablation,<sup>[31]</sup> or into oil lubricants used as solid additives<sup>[32]</sup> and even external dry lubricating agent.<sup>[33,34]</sup> For example, numerous studies aimed to improve the tribological performance of less lubricating substrates via laser texturing reservoirs which were further burished with WS<sub>2</sub> or MoS<sub>2</sub>.<sup>[35–37]</sup> The underlying objective of the texturing techniques is to precisely fabricate micrometer-scaled tiny dimples that serve as hydrodynamic bearings, reservoirs of lubricant or even as a sink to capture the wear debris. Oksanen et al.<sup>[33]</sup> claimed that it is inefficient to texture a diamond-like carbon (DLC) coated surface, instead only the indirectly treated samples were reliably associated with good tribological tests; therefore, they instead explored WS<sub>2</sub> additions on the laser surface textured hard tetrahedral amorphous carbon (ta-C) films. Cavaleiro and co-workers<sup>[38]</sup> investigated the influence of rough surface patterning on the triboperformance of W–S–C–Cr coatings and found that some deep grooves on coating surface may even contribute to lubrication. However, this study did not unravel the details of the microstructure evolution of the triboinduced WS<sub>2</sub> films inside the grooves.

In wear process, a tribofilm formed during frictional sliding can act as a self-lubricating buffer layer to isolate the metal-to-metal direct contact. It is noteworthy that, on the one hand, pure WS<sub>2</sub> is rather soft, yet porous subjecting to oxidation in moisture and thereby diminishing the lubricative properties.<sup>[39]</sup> On the other hand, high resolution transmission electron microscopy (HR-TEM) observations of tribofilms in situ at the wear track by focused ion beam (FIB) slicing have revealed subsurface reorientation of flexible WS<sub>2</sub> nanoplatelets, with their (002) basal planes rearranged parallel to the coating surface into the so-called “frictionless” direction.<sup>[40]</sup> The latter confirms that soft WS<sub>2</sub> can self-adapt itself to reorientate during a sliding contact.<sup>[21,41]</sup>

Therefore, apart from providing lubrication, the soft mechanical response of WS<sub>2</sub> also inspires us to further take advantage of the reoriented WS<sub>2</sub> tribofilms as “patches” to simultaneously heal microcracks occurring in the coatings. This approach sets aside from the standard idea of producing an “ideal” coating by focusing instead on the exploration of a self-healing and self-adaptive tribosystem. Our hypothesis is that during sliding contact with the counterpart, the wear debris is compacted and transformed into a closed continuous tribofilm, which “self-repairs” the damage near the sliding surface.

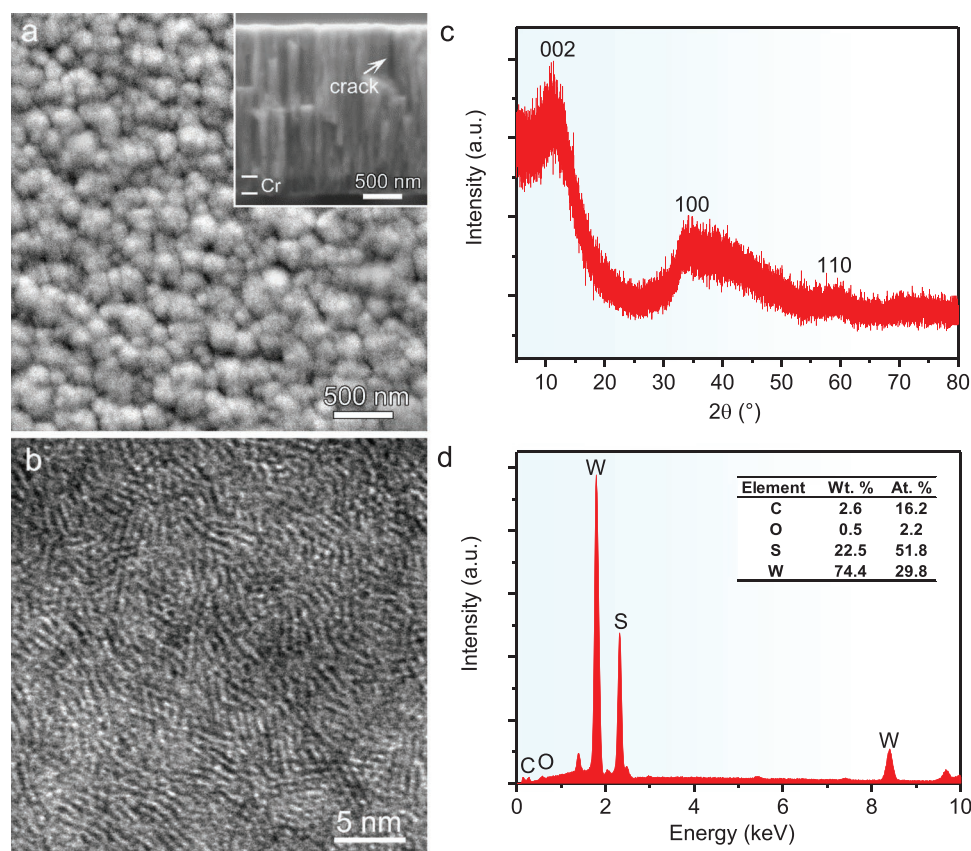


**Figure 1.** Characterizations of magnetron sputtered WS<sub>2</sub>/a-C coating: a) top-view SEM observation with the inset showing the columnar structure on fractured cross-section where an arrow indicating potential cracks along the columnar boundary; b) HR-TEM image revealing randomly orientated short WS<sub>2</sub> nanoplatelets embedded in an amorphous carbon matrix; c) GI-XRD spectrum of the coating; and d) indicative EDS composition.



## 2. Results and Discussion

### 2.1. Microstructure Characterization

The scanning electron microscopy (SEM) image in **Figure 1a** shows that the pristine  $WS_2/a-C$  coating exhibits a domed surface morphology, which is characteristic of magnetron sputtered coatings. The fractured cross section in the inset reveals that the coating has a columnar structure. The column boundaries may be preferential cracking paths and potentially induce coating failure in applications. HR-TEM image in **Figure 1b** reveals that short  $WS_2$  nanoplatelets (<5 nm in length) are randomly embedded in an a-C matrix. The amorphous state is further confirmed by the grazing incidence X-ray diffraction (GI-XRD) spectrum as shown in **Figure 1c**, where a broad shoulder peak around  $WS_2$  (100) is observed. The XRD spectrum also indicates that the  $WS_2$  (002) basal plane located at  $2\theta \approx 12^\circ$  is more or less consistent with the JCPDS card (No. 008-0237), although the peak has a slight shift toward a lower diffraction angle (e.g., from  $\approx 14^\circ$  in the standard diffraction down to  $12^\circ$ ). This is reasonable because carbon incorporation from  $WS_2/a-C$  nanocomposite increases the lattice parameters of  $WS_2$  (002) planes.<sup>[9,41]</sup> Note that the residual stress in the coating may also influence their lattice parameter. The energy dispersive X-ray spectroscopy (EDS) spectrum in **Figure 1d** quantifies the chemical composition of the present coating roughly as 16C–52S–30W–2O (at%). The S/W ratio of  $\approx 1.7$  implies certain sulfur deficiencies as previously reported in the sputtered  $WS_2$ -based coatings due to the preferential resputtering of sulfur.<sup>[9]</sup> More details about the microstructure and mechanical properties of the coatings were given in our previous work.<sup>[9,39,40]</sup>

### 2.2. Self-Healing of Damage

**Figure 2a** shows the notched coating by scratching. As can be seen, the coating has a dimple-like delamination of a width as large as  $\approx 45 \mu\text{m}$ . The overlaid EDS elemental mapping is shown in **Figure 2b**. In the central part of delaminated dimples strong signal of Si from the substrate (colored in white), and Cr from the interlayer (colored in cyan) along the rim of delaminated dimples are detected in contrast to the mixed appearance of S (colored in red), W (colored in blue) and C (colored in purple) from the pristine coating as presented in the two sides of the notched damage. This suggests a complete localized failure of the coating. The closeup in **Figure 1c** further confirms failure of the coating and delamination, which were preintroduced to mimic severe damage of the coating during practical use. Such damage may include catastrophic events and break-down due to accumulated fatigue in the subsurface area.

To check the self-healing capacity of the investigated coating, a set of in situ tribotests were performed, and the wear track was checked by SEM and EDS after sliding in dry air for 100, 500, 2000, and 6000 laps, respectively. SEM morphology and overlaid EDS mapping of the wear track are presented in **Figure 3**. **Figure 3a** shows that, although a large number of cracks still remain, 100 laps sliding already results in a large portion of the delaminated spots being healed as evidenced by the disappearance of the Cr and Si signals from **Figure 3a**.

A comparison of **Figure 3a** with the overlaid EDS mapping of **Figure 2b** and detailed element mappings in **Figure 4a1–a6, b1–b6** confirm that a tribofilm is formed and is transferred to the voids. In particular, the sulfur and tungsten elements are traced, whereas there is also some oxygen traceable along the wear track. **Figure 4b5, b6** also shows that the intensities of Cr and Si are weakened due to the shielding of tribofilm filled in the notch as compared to that in **Figure 4a5, a6**, respectively, where Cr and Si fully cover the whole dimple-like damage.

After 500 laps sliding, the large residue voids are almost repaired, as the Si signal in the EDS of **Figure 4c6** has almost disappeared. Meanwhile, the oxygen seems to spread further forward along the sliding direction, indicating the occurrence of oxidation at the sliding interface. Sliding for 2000 laps results in a full healing of the damage. **Figure 3c** shows continuous and dense tribofilms cover the voids entirely. This healing is confirmed by **Figure 4d1–d6** where the EDS mappings trace the element transport, and in particular the distribution of tungsten and carbon are uniform and nearly indistinguishable

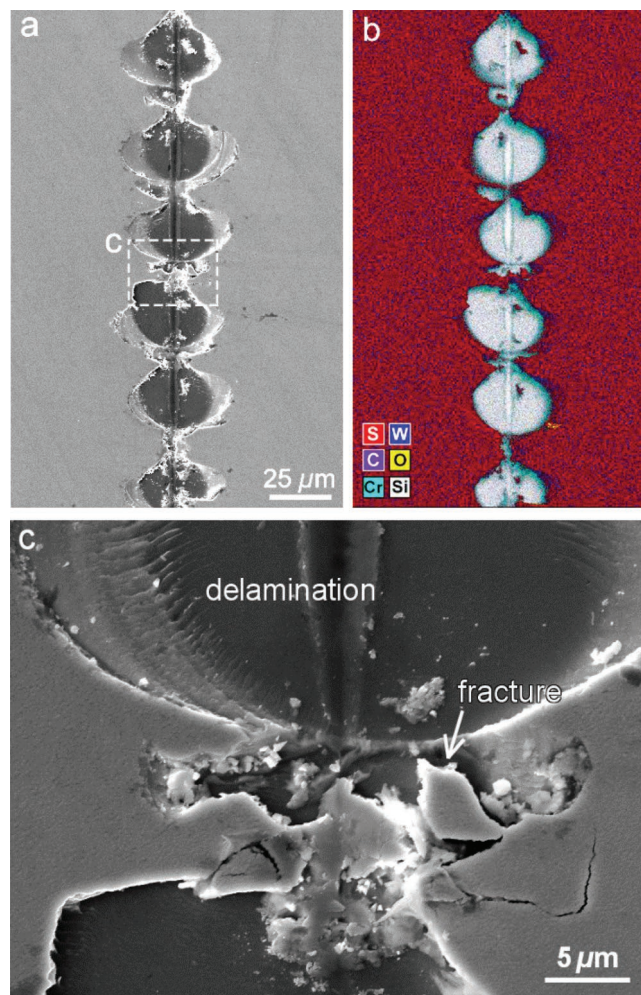


**Figure 2.** a,b) SEM observation and overlaid EDS elemental mapping of the prenotch damaged coating; c) close-up of the marked area in (a) indicating coating fracture and complete delamination to simulate service damage.



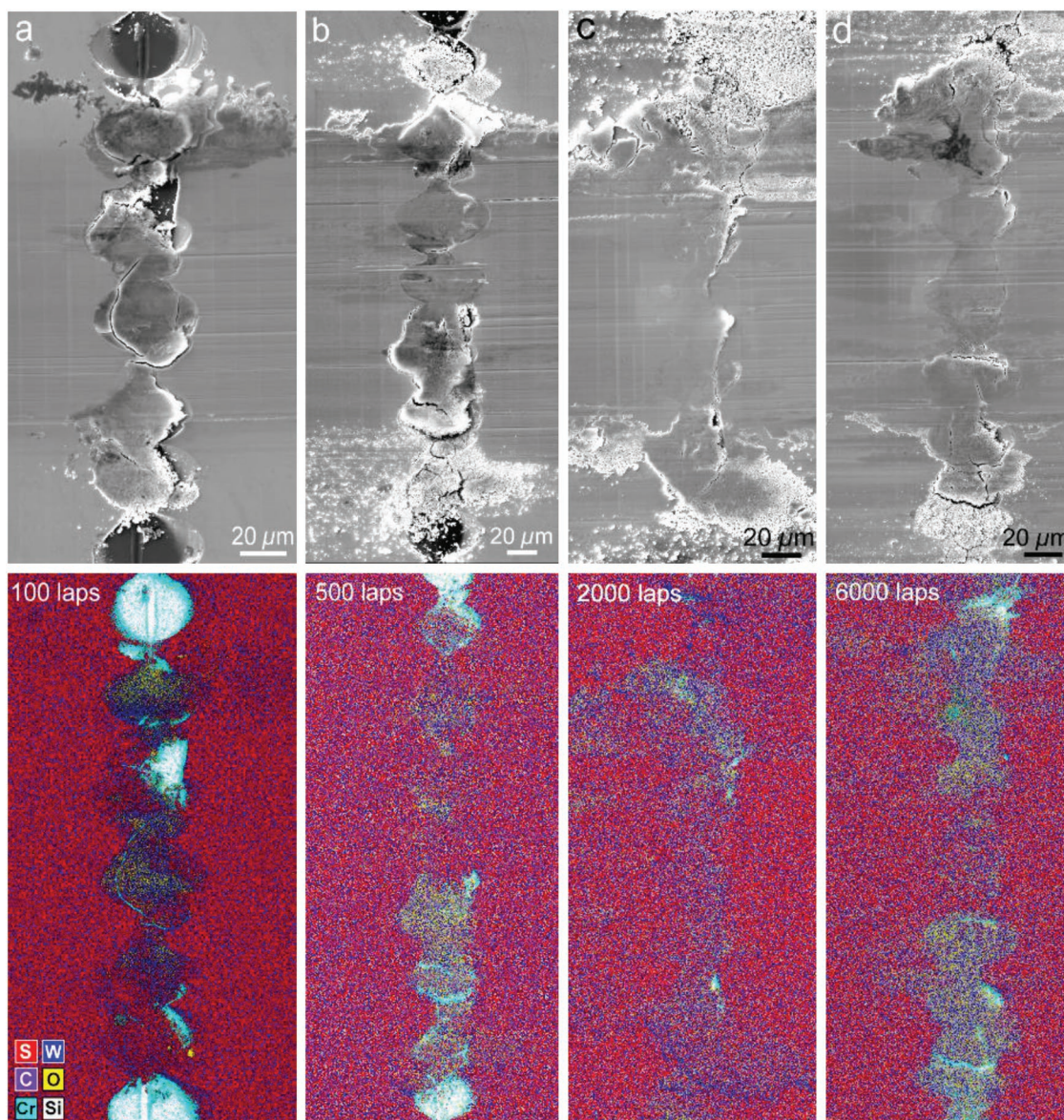


**Figure 3.** SEM micrographs (top) and overlaid EDS elements mapping (bottom) showing the self-healing process of damage after sliding 100, 500, 2000, and 6000 laps, respectively.

across the original coating and the healed notch part. This suggests that the notched damage has been successfully patched by the tribofilm that was transferred toward the damage sites, triggering the subsequent local healing. In addition, the intensity of Si completely disappeared, suggesting a gradual overlayer built-up onto the top of the damage, indicating a full recovery.

**Figure 5a** presents a comparison of the transverse profiles of the notched damage before and after healing, where the initial notch was around 1.8 μm deep and 45 μm wide. After tribosliding induced healing, the notch is filled up and presents a flattened top surface morphology. In line with the cross-section profiles, linear EDS scans of the relevant elements across the notch are performed. **Figure 5b** shows a rather steep decrease in the content of W and S where the notched damage is located, together with an obvious rise in the content of Cr and Si.

In particular, the sharp peak of Si at the center indicates the removal of substrate material by scratching. In contrast, after healing by 6000 laps sliding, the signals of Cr and Si basically disappear because they are submerged under the upper filled materials. Apart from certain increase in O and only a partial recovery of S as shown in **Figure 5c**, the signals of tungsten and carbon hardly change over the outside of the pristine coating passing through the healed notch. As a consequence, EDS reconfirms that the elements of W, S, and C are indeed transported into the notch and trigger the repairing processes. Note that O is introduced by oxidation, which is more likely occurring on the counterface when the worn film is stored and exposed to oxygen which then get intermixed during the sliding/healing process. This explains the higher content of O in the tribofilm than that of the original film.



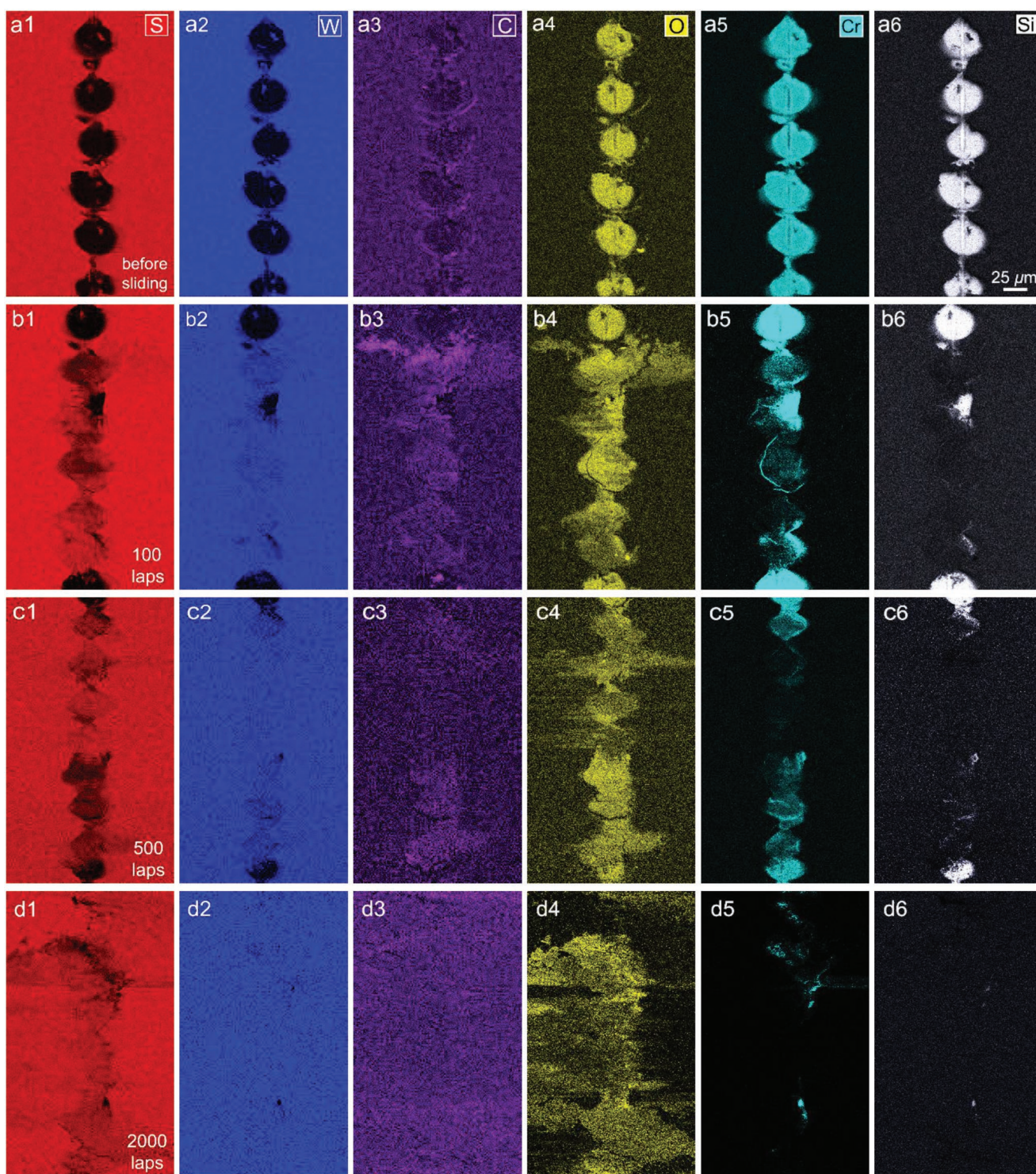


**Figure 4.** Detailed EDS mapping of individual elements during the healing process: a) notched sample before sliding, and after sliding for b) 100 laps, c) 500 laps, and d) 2000 laps, respectively. The associated number 1–6 refers to the element of S, W, C, O, Cr, and Si, respectively. Note there is a slight shift of the wear track after each interruption.

To unravel the self-healing process, SEM observations at different stages and locations of the wear track are investigated in **Figure 6**. Figure 6a shows that one dimple-like pit at the edge of wear track after sliding 500 laps has accumulated and therefore

could store a substantial amount of wear debris. The very tiny particles as seen at high magnification in Figure 6b generally originate from the removal of the domed protuberances (see Figure 1a) of typical PVD coating during wear. At the same



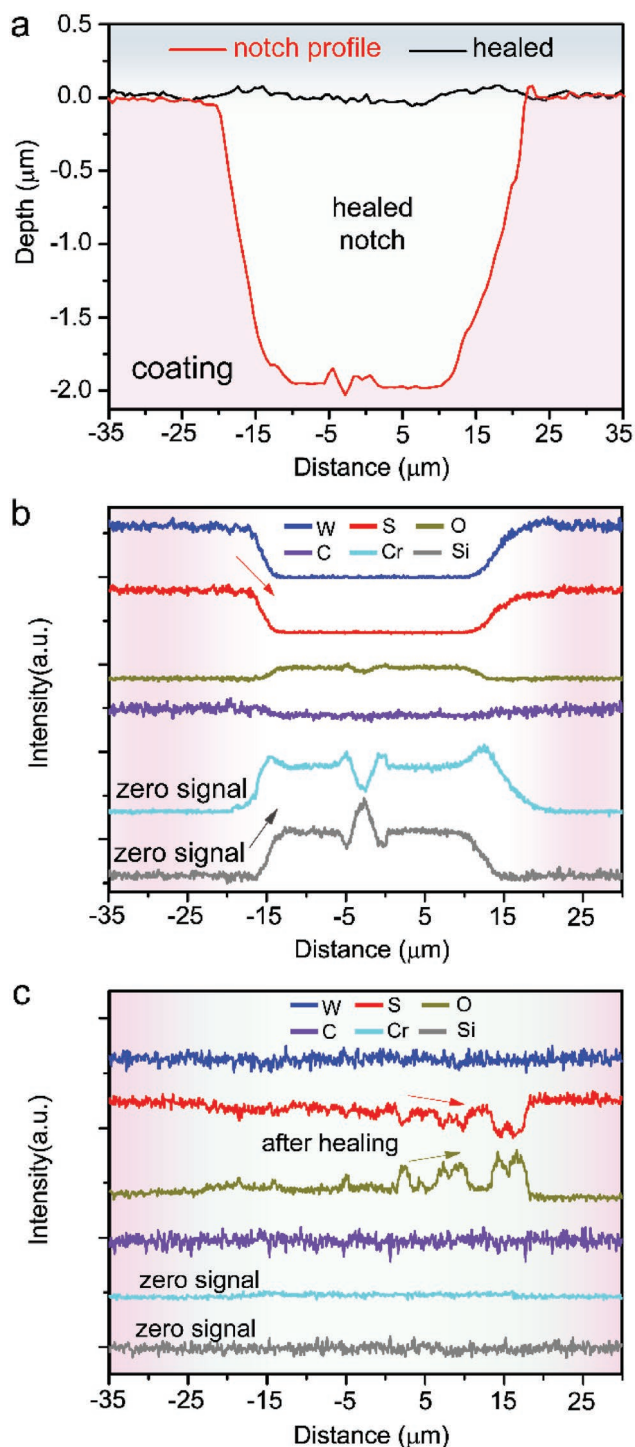


**Figure 5.** Optical confocal morphologic profiles a) and linear EDS compositional profiles across the notched damage before b) and after c) healing by sliding 6000 laps, respectively.

stage toward the inner side of the wear track, the debris, under sliding stimuli and loading pressure, are continuously filled into the notch as shown in Figure 6c,d. Later the debris is connected and flattened until dense and continuous tribofilms are successfully formed. As a consequence, the damaged notch after sliding

6000 laps is restored by the filled tribofilm to various extents as shown in Figure 6e. The closer view in Figure 6f of the marked area in Figure 6e confirms a full repair, at least locally. It is noteworthy that continuous tribofilms (as long as tens of microns) can be formed, exhibiting the capability to cover the whole wear track and thus heal over wide damage areas. Also the tribofilm may grow to a certain thickness due to the gradual layer-by-layer built-up (see Figure 6g,h at the stage of 2000 laps).

Atomic force microscope (AFM) was further employed to compare the surface morphology of raw  $WS_2/a-C$  coatings, tribofilm both on the wear track and healed part at nanoscale, respectively. **Figure 7a** indicates that the raw  $WS_2/a-C$  coating has a clear domed-like morphology with a high root mean square roughness ( $R_q$ ) of around 6.8 nm. In contrast, after the sliding process, the wear track is smoother in comparison to the raw coating, as confirmed with a lower  $R_q = 2.2$  nm as shown in Figure 7b. Similar sliding induced smoothing was also reported in a TiC/a-C nanocomposite coating.<sup>[42]</sup> The cross-section profiles of the two throughout line scans (L1 and L2) in Figure 7a,b also confirm the variations in roughness where L1 in the raw coating apparently fluctuates, and the latter is much flattened. This is so because during the sliding process, the peaks of the surface asperities on the rough coating are truncated, leading to a rather flat and polished surface.<sup>[42]</sup> AFM image in Figure 7c, corresponding to the view in Figure 6f, indicates some pile-up at the interface of the tribofilm/healed part, and L3 in Figure 7d confirms that on the healed part, there is a 35 nm thick protuberance above the normal tribofilm on the left of the notch. This indicates that some compaction of the softened tribofilm occurs during the sliding process.

In terms of the tribological performance, the on-going CoF of four tests by sliding 100, 500, 2000, and 6000 laps is presented in **Figure 8**, with the corresponding insets showing the scar morphology of the counterpart ball. Note that after each interrupted test, the ball was checked by OM and then placed at the same position for continued tests. At the onset of the first 100 laps of a running-in period (Figure 8a), the coating starts with a CoF of 0.1. The CoF peaks at about 0.14, and thereafter it fluctuates around a value of 0.075. Figure 8a reveals that a transfer film is formed on the scar of the ball counterpart. However, the transfer film is island-like and distributed dispersedly, indicating that some local areas of ball scar contact with the lubricating tribofilm, while other local areas are still partially in contact with the original raw coating (similarly to a boundary lubrication state in the Stribeck curve with many residue micro-asperities of high surface points). This explains the fluctuations of CoF yet at a relatively high value in the running-in period.

For the second round of tribotest, from 101 to 500 laps, a gradual decrease of CoF down to 0.05 is observed, with an average CoF value of 0.057 for the whole period. This decrease is confirmed by the formation of an almost fully covered transfer film on the wear scar of the ball counterpart as indicated in the inset of Figure 8b. Similarly, the CoF continues to decrease as the sliding laps increase, with a mean value of 0.035 in the period of 501–2000 laps and 0.027 in sliding 2001–6000 laps, respectively. It should be noted that at the restarting of each tribotest, there is always a new running-in period; in fact, the initial CoF of a later test cannot exactly continue the ultralow state of the previous one. However, the running-in period is shortened for later tribotests. For instance,



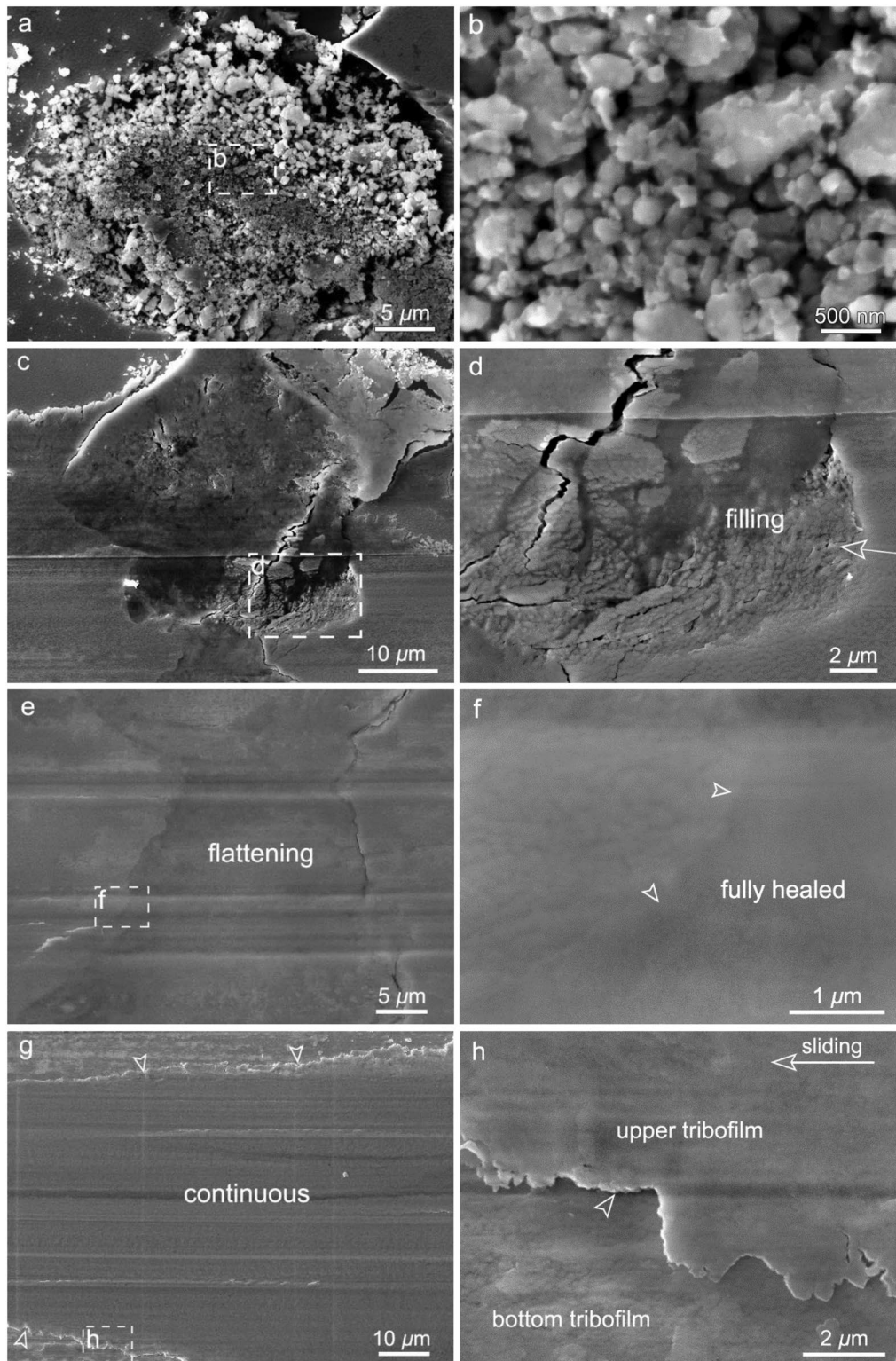


**Figure 6.** Closeups of the self-healing behaviors in the wear track: a,b) a large notched damage accumulates wear debris; c,d) particulate debris are bonded and gradually form a continuous layer; e,f) the notched damage is nearly fully restored by the filled tribofilm, and g,h) layer-by-layer build-up of continuous and thick tribofilms covering the wear track.

Figure 8c,d indicate that it takes around 500 laps for the CoF to reach an ultralow value of  $\approx 0.02$ , while the first run of 500 laps sliding (see Figure 8b) ends up with a relatively high CoF value of

$\approx 0.05$ . This is understandable considering that the preaccumulated tribofilms covering the ball reduce the friction by increasingly disconnecting the direct contact between the steel and coating.

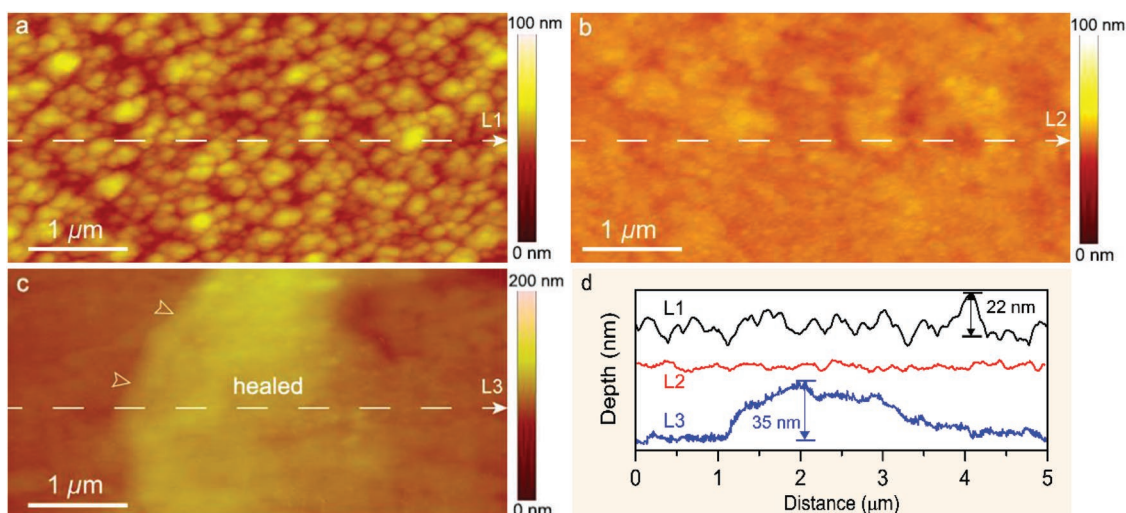


**Figure 7.** AFM of surface topography: a) rough raw  $WS_2/a-C$  coating; b) smoother tribofilm on the wear track; c) pile-up at the interface of tribofilm/healed part in Figure 6f, d) cross-sectional profile of three lines as indicated in (a)–(c).

Another intriguing finding from the apparent changes of the scar morphologies at four stages is that there are many fully colored ripples around the scars shown in the insets of Figure 8b–d. The decreasing diameter of the circular loops from outside to inside indicates that multilayers are accumulated during the sliding process, which is in accordance with the formation of tribofilm on the wear track as shown in Figure 6h. This suggests that  $WS_2$  tribofilms are transferred and aligned continuously throughout the whole wear process.

Note the building-up of transfer film is a dynamic process, i.e., it can be formed, removed, and regenerated simultaneously during the sliding. SEM examination on the ball scar after sliding 6000 laps is shown in Figure 9, and several closeups marked in Figure 9a are presented in Figure 9b–g, respectively. In line with Figure 6a,b, Figure 9b shows that some segmented small debris are worn off from the bulk coating, and then transferred and accumulated ahead of the ball scar. Note that the shear force can slide the basal planes of  $WS_2$  against

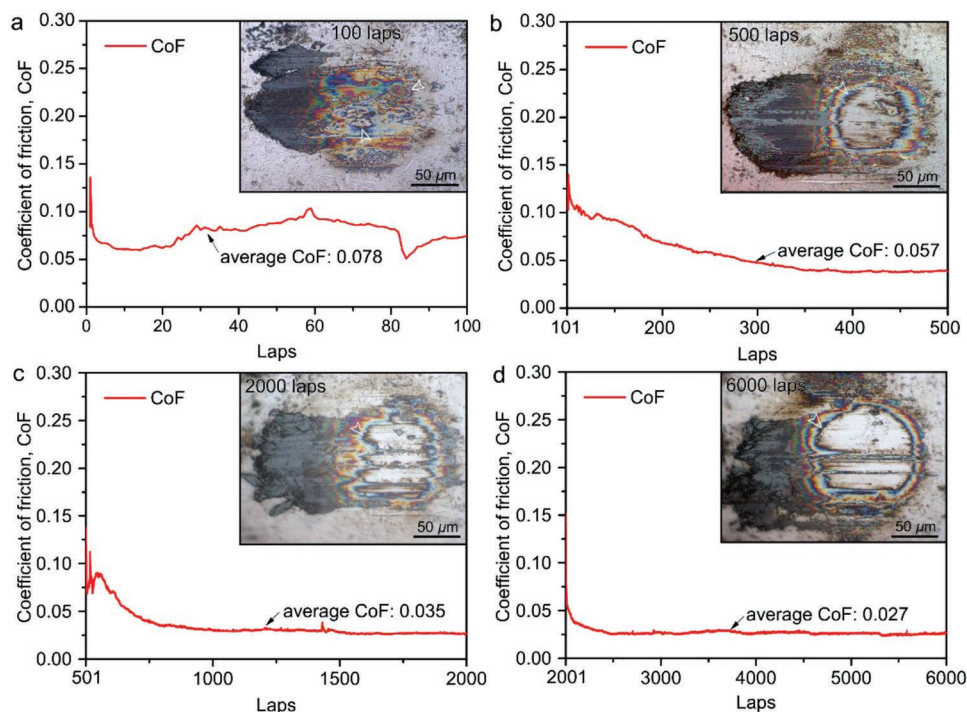


**Figure 8.** Coefficient of friction plot together with inserted OM images showing the corresponding wear scar of ball counterpart: a) after 100 laps; b) after 500 laps; c) after 2000 laps; and d) after 6000 laps. Note that the open arrows pointing at the colorized ripples in the insets indicate the gradual formation of multilayered transfer film.



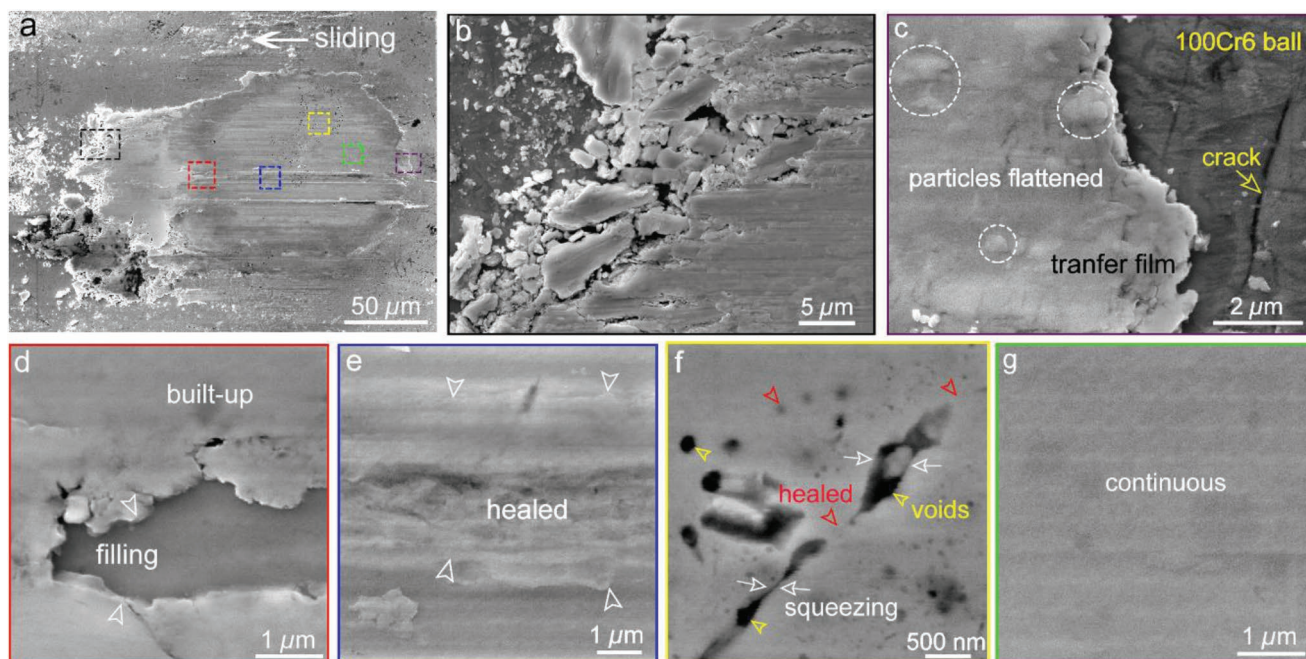


**Figure 9.** Details of the self-healing behavior on the wear scar of counterpart ball after dry air sliding 6000 laps: a) overview of the scar; b) closeups of the marked areas in (a) in corresponding colors showing wear debris accumulated ahead of the scar densifying the transfer film; c) flattened particles; d,e) built-up tribofilm layer by layer; f) squeezed into voids; and g) continuous tribofilms covering the wear scar.

one another by intracrystalline slip and transfer to the rubbing counterface.<sup>[43]</sup> In contrast, at the right side of ball scar (end of contact, see Figure 9c), a dense transfer film, with substantial particles being compacted and flattened, can be observed when compared with the fresh steel ball. Comparison of Figure 9d,e shows the gradual building-up of multilayered transfer film on the ball scar. The tribofilm/transfer film between the coating and counterpart ball can be squeezed to spread out and interconnect (Figure 9e), leading to the self-healing of cracks/damages underneath the tribofilm. Figure 9f further reveals some residual voids (see yellow arrows) exist in the almost flattened transfer film. The white arrows clearly indicate that the transfer films experience some plastic deformation to heal the voids, ultimately resulting in a completely flat and smooth transfer film as seen in Figure 9g. This is comparable with the tribofilm healing the notched damages in the wear track as discussed in Figure 6c–f. Note the squeezed tribofilm and transfer film keep the surfaces of the ball counterpart and the bulk coating apart, leading to a self-lubrication corresponding to an ultralow friction. It should be mentioned that the completely flattened transfer film in the center part of the scar can be very thin as confirmed in EDS mapping shown in Figure 10, where minor S and W elements are traceable in comparison with that at the side edges. This may resort to Auger electron spectroscopy (AES) mapping due to its surface sensitivity for the elemental mapping of such thin layers.<sup>[44]</sup> Previous HR-TEM observations have already confirmed tens of nanometer thick well-aligned TMD tribofilms are transferred onto the wear scar of steel counterpart balls.<sup>[40,43]</sup> The aligned part of the tribofilm hardly grows in thickness too much. This is because once a thin tribolayer is formed, the shear forces become remarkably low, eliminating the driving force for further growth. Consequently,

wear is restricted within this thin buffer layer, which could not transfer shear force sufficiently enough to impose damages to the stronger underneath substrates (coating/steel ball), thus effectively protecting it from further wear.<sup>[45]</sup>

### 2.3. Healing Mechanism

To unravel the healing quality and mechanisms, a cross-section TEM specimen was prepared at a small healed part across the wear track by FIB slicing, more details refer to our earlier work.<sup>[46]</sup> Figure 11a shows a compactly healed notch underneath the Pt protecting layer as indicated. The V-shaped boundary in

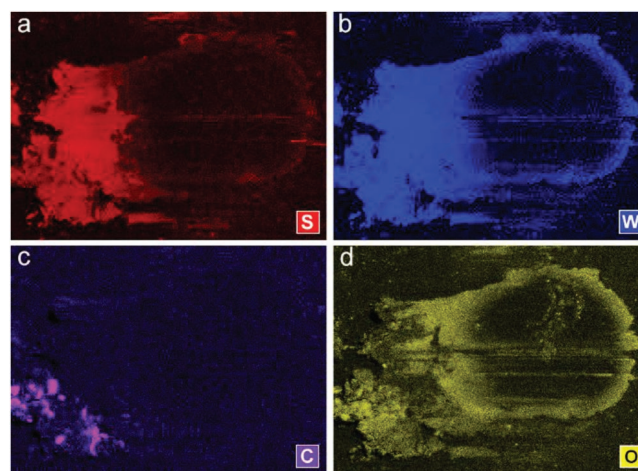


**Figure 10.** Elemental distribution of indicated elements on the wear scar of ball counterpart.



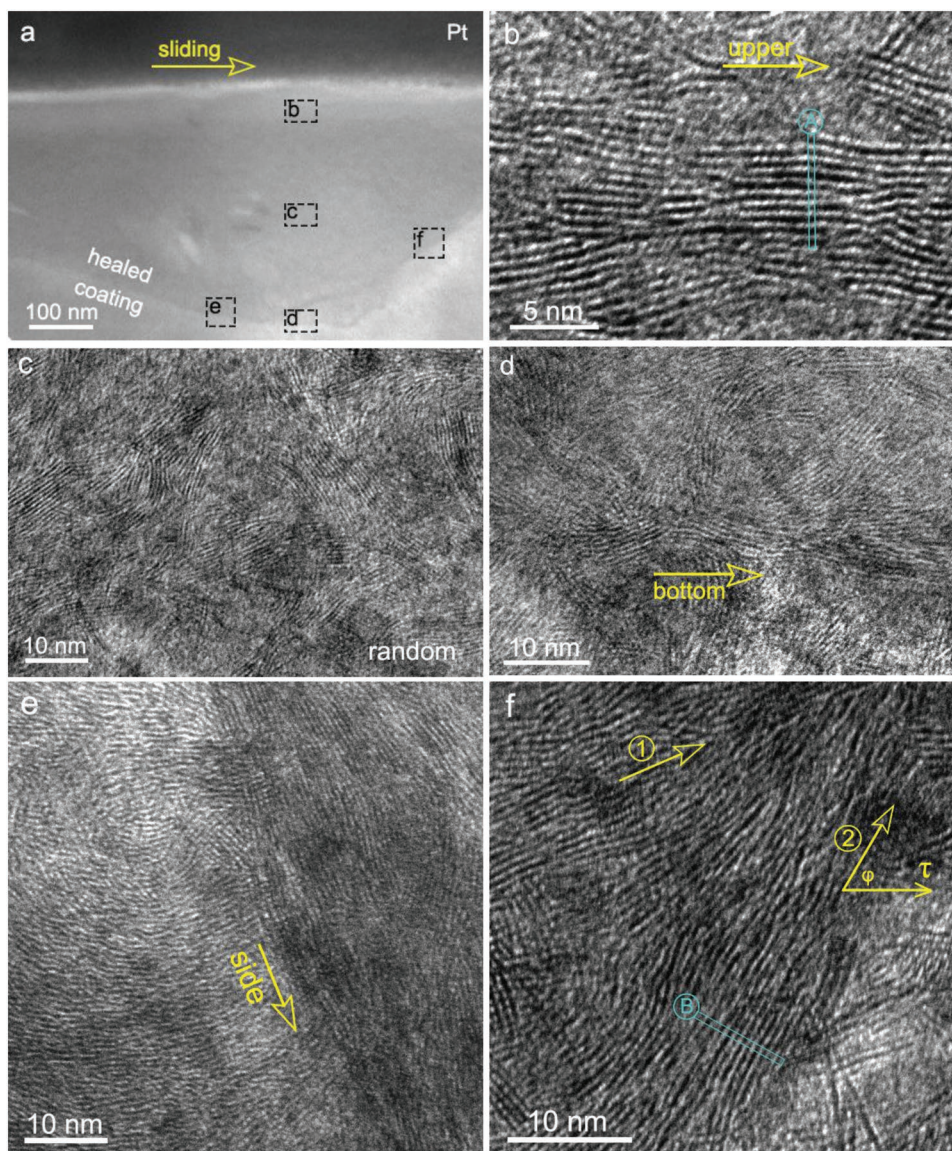


**Figure 11.** TEM confirmation of the healed notch: a) overview; b) HR-TEM image revealing  $\text{WS}_2$  (002) nanoplalets in the upper part of the healed notch to be parallel to the coating surface; c) dense  $\text{WS}_2$  nanoplalets randomized at the middle part of the healed notch; and  $\text{WS}_2$  nanoplalets conformally parallel to the coating/notch interface at d) bottom and e,f) two side areas.

Figure 11a distinguishes the pristine coating (bottom) and the filled tribofilm (upper). This presents a solid proof for the self-healing mechanism in the investigated  $\text{WS}_2/\text{a-C}$  coating. Besides, no cracks neither voids are observed in the entire healed area, pointing to an effective self-healing process. HR-TEM images of Figure 11b–f display some closer views at local regions of the healed notch as marked in Figure 11a. For instance, in the top of the healed part showing in Figure 11b, arresting  $\text{WS}_2$  lamellae are well aligned with (002) basal parallel to the coating surface (i.e., the same to the ball sliding direction). Figure 11c shows that the  $\text{WS}_2$  nanoplalets are highly densified, as compared with that in the original coating as shown in Figure 1b. However, they are rather randomized at the center of the healed notch. At the bottom of the notch, a few  $\text{WS}_2$  nanoplalets are again observed parallel to the bottom of the notch surface (see Figure 11d).

The key question is what is the real driving force for the reorientation of  $\text{WS}_2$  inside the healed notch. It is worth noting that the so-called TMD (002) basal plane reorientation under sliding contact was exclusively reported parallel with the top coating surface;<sup>[30,40,41]</sup> i.e., the “straight” TMD rearrangement is expected to be parallel to the sliding direction of the counterpart ball as shown in Figure 11b. Notwithstanding, an interesting finding in the present study is that  $\text{WS}_2$  nanoplalets are also able to conformally spread over the curved interface. In other words,  $\text{WS}_2$  nanoplalets could align flexibly themselves under shear when they confront with the hard bulk coating (the profile of the notch) as observed in Figure 11e,f. One can easily observe that two directional  $\text{WS}_2$  platelets (see the arrows) converge at the upper right side corner shown in Figure 11f. For instance, the angle ( $\phi$ ) between the localized  $\text{WS}_2$  reorientation

and the top counterpart ball sliding direction as indicated in Figure 11f is  $\approx 45^\circ$  instead of zero. Note that the angle  $\varphi$  changes along the notch surface as its curvature changes. This implies that short randomly oriented  $\text{WS}_2$  nanoplatelets in close proximity can be reoriented and linked to form a closed continuous tribofilm to heal cracks, regardless of the shape provided with the stimuli of the sliding contact. It should also be pointed out that the thickness of perfectly well-aligned  $\text{WS}_2$  nanoplatelets is more than tens nm (Figure 11b,f), much thicker than the reported thickness ( $\approx 5$  nm) as in refs. [29,41,47]. To conclude, TMD basal plane reorientation does not only occur inevitably parallel to the top coating surface under the sliding contact, but also get influenced by the local sliding along with the interface of healed notch during the filling process of tribofilm, which leads to a strong densification.<sup>[30]</sup> Accordingly, such compliance of the tribofilm adds flexibility to heal irregular damage.

To further reveal the local chemical phases and mechanical properties, nanoindentation and Raman spectroscopy analysis were conducted on different zones in the wear track, and their results are shown in Figure 12a–c. Figure 12a illustrates the optical image of a typical healed notch by the tribofilm. The nanohardness and indentation impressions of the tribofilm on the wear track, the healed notch damage and the raw  $\text{WS}_2$ /a-C coating (marked by triangles in respective colors in Figure 12a), together with the pure  $\text{WS}_2$  coating prepared under the same sputtering condition are presented in Figure 12b. It can be seen that the raw  $\text{WS}_2$ /a-C coating has the highest hardness

of  $6.7 \pm 1.5$  GPa, substantially higher than that of the pure sputtered  $\text{WS}_2$  coating of merely  $0.25 \pm 0.05$  GPa. Interestingly, the hardness of the tribofilms both on the wear track and the healed notch part decreases, among which the first is about  $4.3 \pm 1.0$  GPa, almost twice as high as that of the latter ( $2.2 \pm 0.3$  GPa). The hardness differences also shed light on the reason why  $\text{WS}_2$  nanoplatelets tend to flexibly reorientate along the curved interface of the notch and bulk coating (see Figure 11d–f): the healed part mainly consists of soft  $\text{WS}_2$  whereas the bulk coating is much harder; as a result, the frictional force  $F$  drives the reorientation of  $\text{WS}_2$  nanoplatelets first parallel with the sliding direction (arrow 1 in Figure 11f). However, when  $\text{WS}_2$  nanoplatelets interact with harder obstacles, i.e., the inclined ( $\varphi$ ) frontier of the hard raw coatings, they start to deviate from their original direction and instead orientate themselves along the curved interface (arrow 2 in Figure 11f)

$$F = \mu L \quad (1)$$

$$\tau = F/A = F/(\pi D^2/4) = 4 \mu L/\pi D^2 \quad (2)$$

where  $L$  is the normal load (5 N), and  $\mu$  is the measured coefficient of friction (CoF = 0.027 in Figure 8d),  $D$  is the diameter ( $\approx 120 \mu\text{m}$ , see the inset in Figure 8d) of the wear scar of the ball counterpart at the steady-state CoF, and  $\tau$  is the nominal shear stress. Accordingly,  $\tau$  is about 12 MPa over the healing notch. This is much larger than the interfacial shear strength

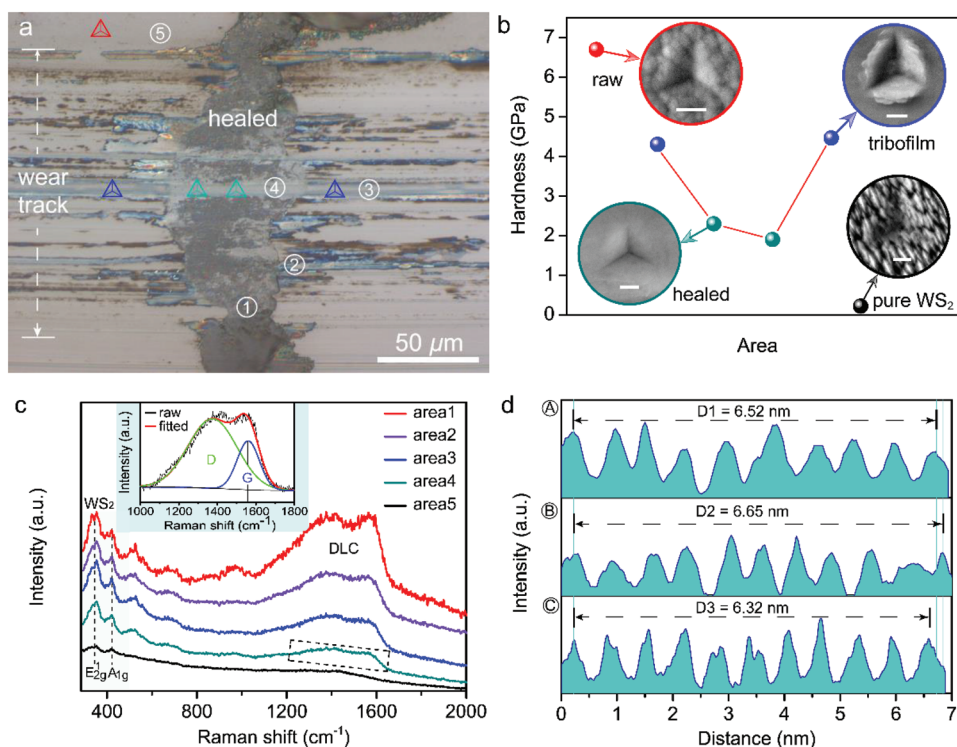


**Figure 12.** a) OM of a typical notch healed by tribofilm; b) hardness and indicative nanoindentation impression of the tribofilm on the wear track and healed notch as marked in (a) as compared to the raw  $\text{WS}_2$ /a-C coating and pure sputtered  $\text{WS}_2$  coating prepared under the same sputtering conditions (all scale bars: 500 nm), respectively; c) Raman spectra of circled areas in (a) with the inset showing typical deconvoluted D and G peaks of diamond-like carbon matrix from the healed part (area 4); d) the distance of ten  $\text{WS}_2$  nanoplatelets in the healed notch with A and B marked in Figure 11b,f, while C is from the  $\text{WS}_2$  target (not shown).



(1–2 MPa) required to drive the WS<sub>2</sub> to cleavage and glide within the hexagonal layers.<sup>[21]</sup> Even along the inclined frontier of the hard bulk coating, the shear stress component can be resolved as  $\tau \times \cos \varphi$  (see Figure 11f), which is still high enough to reorientate the WS<sub>2</sub> nanoplatelets, i.e., the shear stress becomes  $\approx 8.3$  MPa at  $\varphi = 45^\circ$ . It should be mentioned that far away from the direct sliding contact (compare Figure 11b,c), WS<sub>2</sub> nanoplatelets lose the alignment degree of basal planes. This is confirmed by the randomized distribution of TMD in Figure 11c in the middle part of the healed notch and previous results in TMD tribofilms at tens of nanometer away from the sliding interface as reported in refs. [15,29,30,48]. Moser and Lèvy<sup>[30]</sup> found “convective-like” or “turbulent-like” patterns of the basal planes in MoS<sub>2</sub> lubricating films, suggesting the occurrence of relatively easy sliding displacements between localized nanocrystallites in the buffer tribofilm, in accordance with that in the central part of the healed notch (see Figure 11c).

The hardness decrease in the tribofilm is plausibly caused by the release of carbon from the original WS<sub>2</sub>/a-C nanocomposite during the sliding process. It weakens the hardness as the less C content, the closer the chemical coating composition approaches that of pure WS<sub>2</sub>, which is well-known for its extremely low hardness and porous characteristics.<sup>[39,49]</sup> Raman analysis results shown in Figure 12c confirm that apart from clear WS<sub>2</sub> peaks at E<sub>12g</sub> (355 cm<sup>-1</sup>) and A<sub>1g</sub> (421 cm<sup>-1</sup>), the areas 1–4 circled in the wear track of Figure 12a all present the typical amorphous carbon peaks, indicating the existence of carbon in the tribofilm. As an illustration, the Raman shift from 1000 to 1800 cm<sup>-1</sup> in area 4 (the tribofilm on the healed notch) can be deconvoluted into D peak at 1376 cm<sup>-1</sup> and G peak at 1560 cm<sup>-1</sup> of DLC phase. Note that both the peak intensity of WS<sub>2</sub> and a-C are not very strong in the raw bulk coating (area 5), indicating that sliding may help the two phases becoming more Raman-active. The Raman spectra of areas 3–4 confirm similar chemical phases of the tribofilms either on the healed notch (area 4) or on the wear track (area 3). Besides, one can see a gradual increase in the Raman excitation intensity of DLC phase from the center of the wear track to the side edge, which is in accordance with the EDS results of the variation in C content (see Figure 5c) and previous report.<sup>[50]</sup> In addition, we compared the spacing of WS<sub>2</sub>(002) crystalline planes in Figure 12d, it can be determined that the distance of each WS<sub>2</sub> layer in the WS<sub>2</sub> target is about 0.63 nm, while those in the top (Figure 11b) and side zone (Figure 11f) of the healed notch are 0.65–0.66 nm, indicating the distance between the WS<sub>2</sub> layers is expanded. Other intercalants can be readily inserted in between the layers due to the weak interlayer coupling. For instance, Teer<sup>[51]</sup> reported the positioning of titanium atoms between the neighboring sulfur planes in the MoST structure. This can also be supported by the shift of (002) peak to the left of a lower diffraction angle in the GI-XRD of WS<sub>2</sub>/a-C coating as compared with that of the sputtered pure WS<sub>2</sub> coating.<sup>[40]</sup> Based on the Raman analysis, EDS and HR-TEM results, it is suggested that carbon atoms are partially released from the WS<sub>2</sub>/a-C nanocomposite under sliding shear while some carbon atoms are likely filled in between different WS<sub>2</sub> layers although further research is required for the clarification of C intercalant. Such nanocomposite characteristic of the tribofilm overall offers a good combination of ultralow friction and mechanical potency.

It is noteworthy that Figure 4 shows certain content of oxygen at tribofilm either on the healed notch or on the wear track. Comparisons of the selected area electron diffractions (SAED, not shown here) of the tribofilm-healed notch with the bulk WS<sub>2</sub>/a-C coating confirms the WO<sub>3</sub> (002) plane, unravelling that WS<sub>2</sub> was indeed partially oxidized into WO<sub>3</sub> during the sliding. The oxygen passivation of active sites of the edge-orientated WS<sub>2</sub> leads to the formation of WO<sub>3</sub> during wear, which degrades the tribological properties. HR-TEM micrographs in Figure 13 reveal that WO<sub>3</sub> nanosized particles may partially block the alignment of WS<sub>2</sub> nanoplatelets that is favored for ultralow

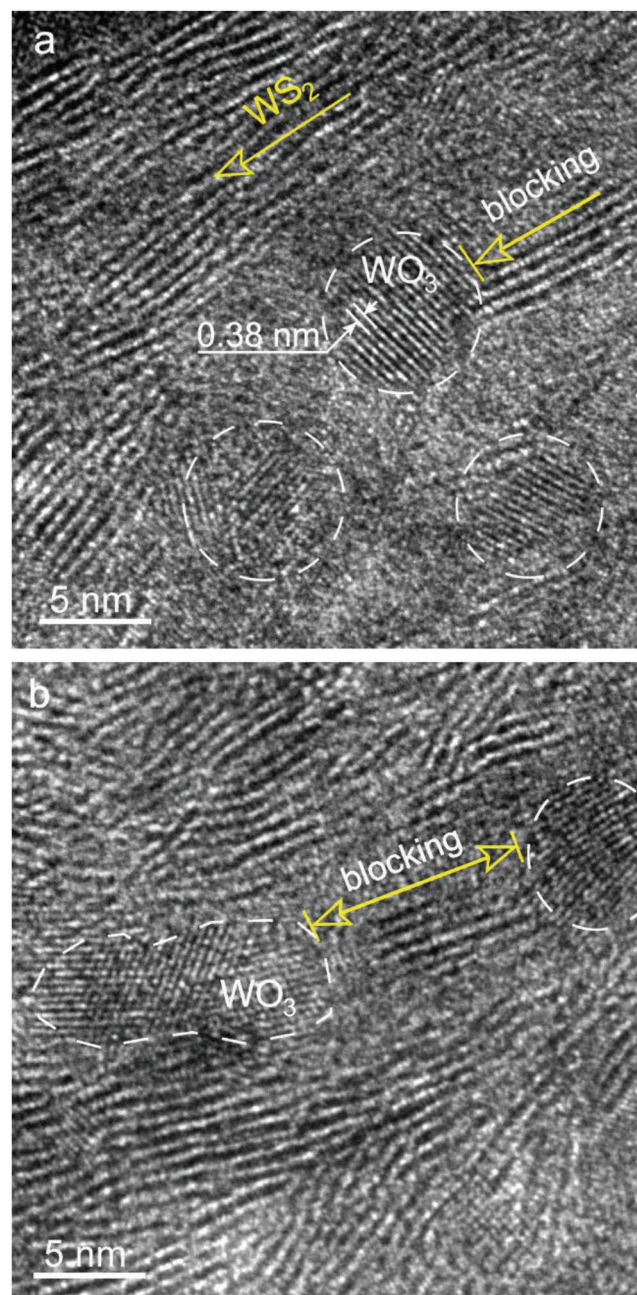


**Figure 13.** HR-TEM showing the blocking effect of WO<sub>3</sub> nanoparticles on the continuous reordering/reorientation of WS<sub>2</sub> nanoplatelets.



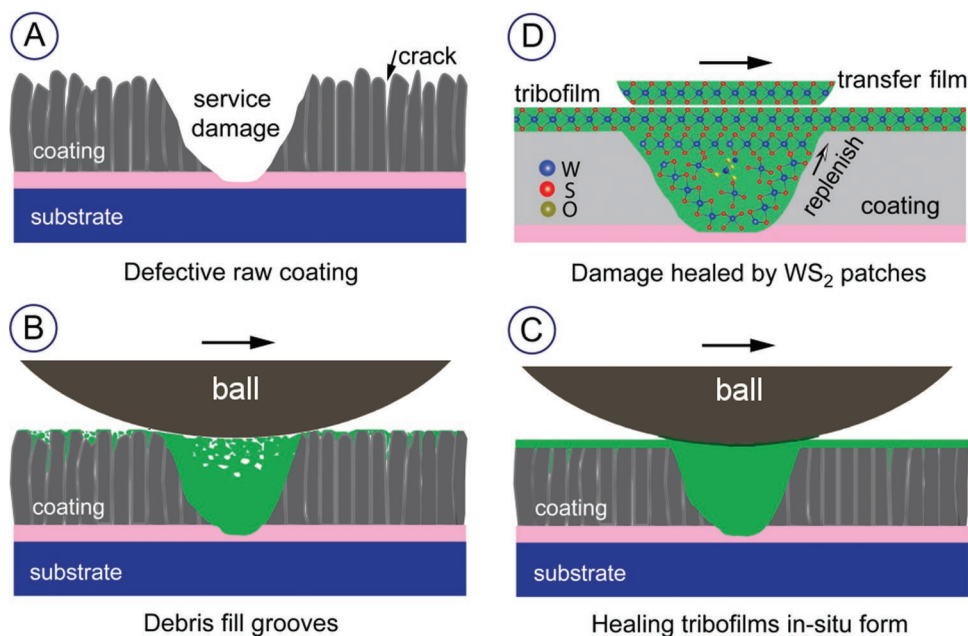


**Figure 14.** Schematic illustration (not in scale) of the in situ self-healing mechanism: a) defective raw coating with aligned voids and cracks along the columnar boundaries and potential damage in service; b) contact sliding ploughs the protuberance of the coating into debris that penetrates into voids/grooves and fills into damage; c) under continuous sliding stimuli the tribofilms form and become flattened, completely patching the damage that reversely act as microreservoirs to replenish superlubricant; d) inside the tribofilm the  $WS_2$  nanoplatelets are reordered, connected, and reoriented with their (002) basal planes parallel to the top coating/the curved surface of the healed-notch. The transfer film and tribofilm self-mate yields interfacial “basal on basal” frictionless sliding.

friction. Nevertheless, the formation of  $WO_3$  nanosized particles hardly influences the healing efficiency as confirmed by Figures 3–6 at micrometer scale.

Figure 14 shows the schematic illustration of the damage self-healing process during the triboactivity of  $WS_2/a-C$  coating. Notably, the damage healing behavior is an approximately spontaneous process, as the damage itself triggers the repairing process without any other external interventions except the stimuli of sliding. Moreover, the healing agent (e.g., tribofilm) derives directly from the raw bulk coating. Such healing is an intrinsic process, which is generally superior to the extrinsic healing avenues, as the later are eventually restrained due to the depletion of externally provided healing agents or their degrading reactions with the matrix) as investigated previously; e.g., depositing lubricating materials into the textured reservoirs of substrates so as to upgrade their triboperformance<sup>[34–36,52]</sup> or alternatively making use of the conformal characteristics of atomic layer deposition to deposit extrinsic upper DLC layers to heal pinholes of some porous coatings.<sup>[53]</sup>

The defective raw coating with cracks at the columnar boundaries and potential damage in services is schematically shown in Figure 14a,b demonstrates that the sliding contact ploughs the asperities of the coating into debris that later penetrate into the intrinsic coating voids or fill into possible service damage. Figure 14c shows under continuous sliding stimuli that the tribofilms form and become flattened and continuous. Meanwhile the  $WS_2$  flakes are transferred to cover the ball counterpart, thereby generating a predominantly self-mated “basal on basal” interfacial sliding as illustrated in Figure 14d. These jointly yield a simultaneous self-healing by recycling of the wear debris

(otherwise wasted) between the mating surfaces and self-lubricating behavior corresponding to a low friction and low wear between the coating and counterpart, as supported by the horizontally aligned  $WS_2$  with frictionless orientation as shown in Figure 11b. Figure 14d reveals that the notched damage serves as microreservoir for storing realigned  $WS_2$  lubricant continuously ready for replenishing frictionless responses. Wang et al.<sup>[34]</sup> controlled the texture of a CrN interlayer to support  $WS_2$  film and found that nanocone array textured  $WS_2$  film exhibited an enhanced lifetime in wear because the regular CrN nanocone arrays serve as favorable reservoirs of  $WS_2$  lubricants.

Therefore, the presence of cracks/damages—common adverse products in tribology—could be restored with beneficial lubricating effects by in situ filling  $WS_2$  tribofilms. As a consequence, we may lift the constraints of preparing ideal coating (e.g., defect free) and rather focus on the self-adaptive and self-repairing system upon the idea to allow the reorientation of hexagonal basal planes flexibly toward the frictionless direction, whereby the “patches” consisting of  $WS_2$  tribofilms heal damage and prolong the lifetime of coated inferior parts.

### 3. Conclusion

This study explored the potential self-healing capability and mechanisms of the  $WS_2/a-C$  tribocoating. In situ formation of triboinduced  $WS_2$  films provides self-healing functionality “patching” voids and repair cracks/damage in the bulk coating. The coating maintains or even enhances its tribological properties because the damage may serve as reservoir storing superlubricant that is transformed from the otherwise

wasted debris. Besides, the flexible compliance of WS<sub>2</sub> nanoplatelets renders tribofilm conformal to the curved interface, indicating its ability to heal complex and irregular shape of damage.

Through intrinsically repairing damage, coatings could promote triboefficiency over time and prevent costs incurred by coating failures. The self-healing capacity of tribofilms thus lifts the constraints of producing ideal coatings for practical triboapplications.

#### 4. Experimental Section

Nanocomposite WS<sub>2</sub>/a-C coatings were deposited on single crystal silicon (100) wafers via a TEER UDP400/4 closed-field unbalanced magnetron sputtering system (CFUMS). The substrates were ultrasonically cleaned in acetone prior to Ar plasma etching for 20 min at a negative bias voltage of 400 V (pulsed direct current, p-DC mode at 250 kHz, 87.5% duty cycle). The nanocomposite coatings were cosputtered from two WS<sub>2</sub> targets (99.9% purity) at an average current of 0.5A (p-DC 150 kHz, 70% duty cycle) and one graphite target (99.9% purity, 0.5 A, direct current mode). The substrates were placed vertically on a carousel holder that was rotated at 3 rpm in front of the targets, without applying additional substrate heating during the deposition. First a thin Cr interlayer 300 nm thick was deposited to facilitate good interfacial adhesion between the coating and substrate. The WS<sub>2</sub>/a-C coatings 1.6–2 μm thick were prepared at an Ar pressure of 0.6 Pa. The deposition time was set to 2 h at a target–substrate distance of 220–290 mm.

A CSM scratch tester equipped with a spherical diamond tip (10 μm in radius) was used to deliberately induce two types of notches, namely, around 2 and 45 μm wide, respectively, onto the coating. The first narrow one (not shown) is for cross-section TEM observations, and the wide one penetrates through the coating until it reaches the Si substrate, which triggers a total coating failure to simulate a potential damage in service. To observe the healing efficiency, a tribotest was interrupted at 100, 500, 2000, and 6000 laps, respectively, for microscopic characterization, employing a CSM ball-on-disk tribometer against a 100Cr6 ball (6 mm in diameter) at a fixed sliding speed of 10 cm s<sup>-1</sup>. The test was performed at room temperature (25 ± 2 °C) and under a normal load of 5 N generating a mean Hertzian contact pressure of ≈0.75 GPa. The wear track diameter was set to 15 mm. The relative humidity (RH) was controlled at 5–7% by a home-made humidity adjuster. After each interrupted test, the wear scar of the steel ball counterpart and the wear track of the coating sample were examined by optical microscopy (OM, Olympus VANOX-T) and SEM (Lyra Tescan) equipped with EDS (EDAX, performed under an accelerating voltage of 20 kV). A confocal microscope (μsurf, NanoFocus) was used to plot the surface morphology of the notch before and after healing by revealing the depth variations. Besides, an AFM (NanoScope 3100) equipped with a Si<sub>3</sub>N<sub>4</sub> tip was utilized in tapping mode to image the surface morphology of raw WS<sub>2</sub>/a-C coatings, tribofilm and healed part at nanoscale. The area of AFM scans was 5 × 5 μm, made with a scan rate of 1 Hz. In addition, an MTS Nano indentation XP equipped with a Berkovich indenter was employed to measure the hardness and modulus of the coatings, formed tribofilm, and healed part, respectively, with a depth-controlled mode of 200 nm. The GI-XRD spectra were conducted at a fixed incident angle of 2° with a PANalytical-X'Pert MRD to characterize the phases in the coatings. Furthermore, the chemical structure and microstructure were scrutinized using Raman spectroscopy (Thorlabs HeNe laser, 632.8 nm wavelength, applied with a power of about 1–2 mW) and HR-TEM (2010F-JEOL, 200 kV). Besides, FIB (Lyra Tescan) was utilized to slice the healed part of a narrow notch and thus prepare TEM lamella. Prior to FIB milling, a thin Pt layer was deposited to protect the specimen from severe Ga ion irradiation damage.

#### Acknowledgements

Financial support by the Key Research and Development Project of Hainan Province, China (ZDYF2019206) and the National Foreign Expert High-end Project (G20190234002) is thanked. H.T.C. acknowledges China Scholarship Council, China for his Ph.D. scholarship (CSC, No. 201406160102). Prof. Wesley Browne from the University of Groningen, the Netherlands is appreciated for his assistance with Raman spectroscopy.

#### Conflict of Interest

The authors declare no conflict of interest.

#### Keywords

basal plane reorientation, damage self-healing, magnetron sputtering deposition, ultralow friction, WS<sub>2</sub>/a-C tribocoating

Received: May 30, 2019

Revised: August 30, 2019

Published online: November 20, 2019

- [1] B. M. D. Hager, P. Greil, C. Leyens, S. van der Zwaag, U. S. Schubert, *Adv. Mater.* **2010**, *22*, 5424.
- [2] S. R. White, N. R. Sottos, P. H. Geubelle, J. S. Moore, M. R. Kessler, S. R. Sriram, E. N. Brown, S. Viswanathan, *Nature* **2001**, *409*, 794.
- [3] B. J. Blaiszik, S. L. B. Kramer, S. C. Olugebefola, J. S. Moore, N. R. Sottos, S. R. White, *Annu. Rev. Mater. Res.* **2010**, *40*, 179.
- [4] S. Joshi, S. Goyal, A. Mukherjee, M. S. Reddy, *J. Ind. Microbiol. Biotechnol.* **2017**, 441511.
- [5] H. M. Jonkers, A. Thijssen, G. Muyzer, O. Copuroglu, E. Schlangen, *Ecol. Eng.* **2010**, *36*, 230.
- [6] H. J. Yang, Y. T. Pei, J. C. Rao, J. T. M. De Hosson, S. B. Li, G. M. Song, *Scr. Mater.* **2011**, *65*, 135.
- [7] H. J. Yang, X. H. Shao, Y. T. Pei, Z. F. Zhang, J. T. M. De Hosson, *Mater. Lett.* **2018**, *227*, 51.
- [8] T. Banerjee, A. K. Chattopadhyay, *Surf. Coat. Technol.* **2014**, *258*, 849.
- [9] H. T. Cao, F. Wen, S. Kumar, P. Rudolf, J. T. M. De Hosson, Y. T. Pei, *Surf. Coat. Technol.* **2019**, *365*, 41.
- [10] F. Lévy, J. Moser, *Surf. Coat. Technol.* **1994**, *68–69*, 433.
- [11] J. Q. Liu, L. J. Li, B. Wei, F. Wen, H. T. Cao, Y. T. Pei, *Surf. Coat. Technol.* **2019**, *365*, 33.
- [12] Y. T. Pei, D. Galvan, J. T. M. De Hosson, *Acta Mater.* **2005**, *53*, 4505.
- [13] T. Polcar, M. Evaristo, A. Cavaleiro, *Plasma Processes Polym.* **2009**, *6*, 417.
- [14] B. Deepthi, H. C. Barshilia, K. S. Rajam, M. S. Konchady, D. M. Pai, J. Sankar, *Tribol. Int.* **2011**, *44*, 1844.
- [15] H. Nyberg, J. Sundberg, E. Särhammar, F. Gustavsson, T. Kubart, T. Nyberg, U. Jansson, S. Jacobson, *Wear* **2013**, *302*, 987.
- [16] K. Yalamanchili, I. C. Schramm, E. Jiménez-Piqué, L. Rogström, F. Mücklich, M. Odén, N. Ghafoor, *Acta Mater.* **2015**, *89*, 22.
- [17] K. Yalamanchili, F. Wang, H. Aboufadel, J. Barrirero, L. Rogström, E. Jiménez-Piqué, F. Mücklich, F. Tasnadi, M. Odén, N. Ghafoor, *Acta Mater.* **2016**, *121*, 396.
- [18] Z. Y. Wang, X. W. Li, X. Wang, S. Cai, P. L. Ke, A. Y. Wang, *Surf. Coat. Technol.* **2016**, *304*, 553.
- [19] Y. Xi, S. Zhang, *Surf. Coat. Technol.* **2014**, *258*, 1.
- [20] Y. T. Pei, C. Q. Chen, K. P. Shaha, J. T. M. De Hosson, J. W. Bradley, S. A. Voronin, M. Cada, *Acta Mater.* **2008**, *56*, 696.
- [21] C. Muratore, A. A. Voevodin, *Annu. Rev. Mater. Res.* **2009**, *39*, 297.

- [22] X. Quan, M. Hu, X. M. Gao, Y. L. Fu, L. J. Weng, D. S. Wang, D. Jiang, J. Y. Sun, *Tribol. Int.* **2016**, 99, 57.
- [23] A. A. Voevodin, J. P. O'Neill, J. S. Zabinski, *Surf. Coat. Technol.* **1999**, 116–119, 36.
- [24] M. Chhowalla, H. S. Shin, G. Eda, L. Li, K. P. Loh, H. Zhang, *Nat. Chem.* **2013**, 5, 263.
- [25] T. W. Scharf, S. V. Prasad, *J. Mater. Sci.* **2013**, 48, 511.
- [26] S. Prasad, J. Zabinski, *Nature* **1997**, 387, 761.
- [27] J. M. Martin, H. Pascal, C. Donnet, T. L. Mogne, J. L. Loubet, T. Epicier, *Surf. Coat. Technol.* **1994**, 68–69, 427.
- [28] T. Onodera, Y. Morita, A. Suzuki, M. Koyama, H. Tsuboi, N. Hatakeyama, A. Endou, H. Takaba, M. Kubo, F. Dassenoy, C. Minfray, L. Joly-Pottuz, J. M. Martin, A. Miyamoto, *J. Phys. Chem. B* **2009**, 113, 16526.
- [29] T. Polcar, M. Evaristo, R. Colaço, C. S. Sandu, A. Cavaleiro, *Acta Mater.* **2008**, 56, 5101.
- [30] J. Moser, F. Lévy, *Thin Solid Films* **1993**, 228, 257.
- [31] A. A. Voevodin, J. S. Zabinski, *Thin Solid Films* **2000**, 370, 223.
- [32] W. Yue, C. Y. Liu, Z. Q. Fu, C. B. Wang, H. P. Huang, J. J. Liu, *Tribol. Int.* **2013**, 62, 117.
- [33] J. Oksanen, T. J. Hakala, S. Tervakangas, P. Laakso, L. Kilpi, H. Ronkainen, J. Koskinen, *Tribol. Int.* **2014**, 70, 94.
- [34] D. S. Wang, M. Hu, D. Jiang, X. M. Gao, Y. L. Fu, Q. Q. Wang, J. Yang, J. Y. Sun, L. J. Weng, *Mater. Lett.* **2017**, 188, 267.
- [35] A. A. Voevodin, J. S. Zabinski, *Wear* **2006**, 261, 1285.
- [36] Y. S. Lian, H. F. Chen, J. X. Deng, B. Yao, D. X. Deng, S. T. Lei, *Int. J. Refract. Hard Met.* **2018**, 72, 286.
- [37] T. C. Hu, Y. S. Zhang, L. T. Hu, *Wear* **2012**, 278–279, 77.
- [38] J. V. Pimentel, M. Danek, T. Polcar, A. Cavaleiro, *Tribol. Int.* **2014**, 69, 77.
- [39] H. T. Cao, J. T. M. De Hosson, Y. T. Pei, *Surf. Coat. Technol.* **2017**, 332, 142.
- [40] H. T. Cao, F. Wen, J. T. M. De Hosson, Y. T. Pei, *Mater. Lett.* **2018**, 229, 64.
- [41] J. Sundberg, H. Nyberg, E. Särhammar, F. Gustavsson, T. Kubart, T. Nyberg, S. Jacobson, U. Jansson, *Surf. Coat. Technol.* **2013**, 232, 340.
- [42] K. P. Shaha, Y. T. Pei, D. Martinez-Martinez, J. T. M. De Hosson, *Surf. Coat. Technol.* **2010**, 205, 2624.
- [43] T. W. Scharf, P. G. Kotula, S. V. Prasad, *Acta Mater.* **2010**, 58, 4100.
- [44] J. M. Martin, T. Le Mogne, M. Boehm, C. Grossiord, *Tribol. Int.* **1999**, 32, 617.
- [45] F. Gustavsson, S. Jacobson, *Tribol. Int.* **2016**, 101, 340.
- [46] H. T. Cao, J. T. M. De Hosson, Y. T. Pei, *Mater. Res. Lett.* **2019**, 7, 103.
- [47] N. Takahashi, S. Kashiwaya, *Wear* **1997**, 206, 8.
- [48] J. Moser, F. Levy, *J. Mater. Res.* **1992**, 7, 734.
- [49] J. Xu, L. Q. Chai, L. Qiao, T. F. He, P. Wang, *Appl. Surf. Sci.* **2016**, 364, 249.
- [50] T. Polcar, M. Evaristo, A. Cavaleiro, *Plasma Processes Polym.* **2007**, 4, S541.
- [51] D. G. Teer, *Wear* **2001**, 251, 1068.
- [52] Z. Wu, Y. Q. Xing, P. Huang, L. Liu, *Surf. Coat. Technol.* **2017**, 309, 21.
- [53] E. Härkönen, I. Kolve, B. Díaz, J. Światowska, V. Maurice, A. Seyeux, P. Marcus, M. Fenker, L. Toth, G. Radnoczi, M. Vehkamäki, M. Ritala, *ACS Appl. Mater. Interfaces* **2014**, 6, 1893.